Top-down fabricated silicon nanowire sensors for real-time chemical detection

2010 Nanotechnology 21 015501

(http://iopscience.iop.org/0957-4484/21/1/015501)

Nanotechnology **21** (2010) 015501 (9pp) doi:10.1088/0957-4484/21/1/015501

Top-down fabricated silicon nanowire sensors for real-time chemical detection

Inkyu Park[1,4], **Zhiyong Li**[2], **Albert P Pisano**[3] **and R Stanley Williams**[2]

[1] Department of Mechanical Engineering, Korea Advanced Institute of Science and Technology (KAIST), Daejon, 305-701, Korea
[2] Information and Quantum System Lab, Hewlett-Packard Laboratories, Palo Alto, CA 94304, USA
[3] Berkeley Sensor and Actuator Center and Department of Mechanical Engineering, University of California at Berkeley, Berkeley, CA 94720, USA

E-mail: inkyu.park@kaist.ac.kr

Received 28 July 2009, in final form 26 October 2009
Published 30 November 2009
Online at stacks.iop.org/Nano/21/015501

Abstract
Silicon nanowire (SiNW) sensors have been developed by using top-down fabrication that is CMOS (complementary metal–oxide–semiconductor) compatible for resistive chemical detection with fast response and high sensitivity. Top-down fabrication by electron beam lithography and reactive ion etching of a silicon on insulator (SOI) substrate enables compatibility with the CMOS fabrication process, accurate alignment with other electrical components, flexible design of the nanowire geometry and good control of the electrical characteristics. The SiNW sensors showed a large operation range for pH detection (pH = 4–10) with an average sensitivity of $(\Delta R/R)/\text{pH} = 2.6\%/\text{pH}$ and a rise time of 8 s. A small pH level difference ($\Delta\text{pH} = 0.2$) near neutral pH conditions (pH = 7) could be resolved with the SiNW sensors. The sensor response to the presence of alkali metal ions and the long term drifting effects were also investigated.

(Some figures in this article are in colour only in the electronic version)

1. Introduction

The high surface to volume ratio and small dimensions of nanowires permit rapid depletion and accumulation of charge carriers within their structures, and render them highly sensitive to biological and chemical molecules. Various materials including polymers (e.g. PEDOT, polyaniline and polypyrrole) [1–3], metal oxides (e.g. ZnO, In_2O_3 and SnO_2) [4–6], and silicon [7–10] have been used as materials for producing nanowires. Among these, silicon (Si) is the most common material for nanowire-based sensor use [9–14], particularly in the detection of biomolecules. It has a well-established fabrication process, easy control of electrical properties, facile surface functionalization with chemical linkers and biomolecules, and mechanical and chemical robustness for extended periods of usage.

Although excellent performance of nanowire sensors for the chemical and biological detection devices has been demonstrated [5, 6, 13], the integration of bottom-up grown nanowires with other microfabricated electronic circuits is still a great challenge. In many cases, researchers still utilize deposition of a liquid suspension of multiple nanowires on the pre-fabricated electrodes [15]. Others are developing methods such as using microfluidic channels [16], dielectrophoresis [17], microcontact printing [18], optical trapping [19], and MEMS tweezers [20]. However, these approaches do not guarantee the reproducibility and robustness of the mechanical and electrical contacts. An alternative solution is to use lithographically defined nanowires via a top-down approach. Elibol *et al* [21] fabricated SiNW-like structures (width of 40 nm, thickness of 7 nm) by using confined lateral selective epitaxial growth (CLSEG) within a confined space defined by photolithography. However, the nanowire-like structure fabricated by this approach had poor geometry with large line edge roughness (LER) and low spatial density. Furthermore, accurate control of the electrical properties was not easy. We have previously reported

[4] Author to whom any correspondence should be addressed.

on SiNW sensors fabricated by a CMOS-compatible top-down approach using electron beam lithography and reactive ion etching [9–12]. This top-down approach enabled much more precise control of the geometry and electrical properties of SiNWs and accurate alignment with other electrical components than the bottom-up methods. Reproducible fabrication of SiNWs down to 40 nm width is feasible in any desired geometries via the design flexibility of electron beam lithography. Furthermore, a larger metal–silicon contact area connected seamlessly to SiNWs by electron beam lithography design facilitated minimized contact resistance between metal interconnections and SiNWs, enabling a good ohmic contact. Another advantage of top-down fabricated SiNWs is that they can be easily integrated in a high density array and so novel applications such as chemical mapping (e.g. extracellular biomolecule monitoring from single cells) with nanoscale spatial resolution are possible.

However, in our previous reports [9–12], the geometrical and electrical characterization of the fabricated SiNWs and their sensing performance in areas such as pH level detection, alkali metal ion sensitivity, and long term stability have not been addressed in detail. In this paper, we will report on the following aspects in depth: firstly, geometrical characteristics such as the linewidth (LW) and line edge roughness (LER) of SiNWs will be discussed. Secondly, electrical characteristics and the thermal annealing effect of SiNWs will be addressed. Thirdly, the performance of SiNW sensors in the detection of chemical species properties such as the pH level will be explained. Lastly, the sensitivity to alkali metal ions and the long term stability of SiNW sensors will be investigated.

2. Experimental procedures

Each SiNW sensor was fabricated by a top-down method with electron beam lithography (EBL) for the nanopatterning of SiNW features and reactive ion etching (RIE) for the pattern transfer to the thin silicon (Si) device layer of the silicon on insulator (SOI) substrate. Details of the fabrication procedure are provided as follows.

(1) The 100 nm thick (100) silicon (Si) device layer of the SOI wafer was oxidized to form an oxide of 110 nm thickness via dry thermal oxidation. Then, the silicon device layer was doped with boron (B) by ion implantation (dose $= 1.2 \times 10^{14}$ cm^{-2}, ion energy $= 35$ keV, tilt angle $= 7°$) followed by rapid thermal annealing at 984 °C for 20 s dwelling period in an argon (Ar) environment. This processing condition was used for the average boron concentration of 5×10^{18} cm^{-3} within the silicon nanowire. Afterward, the oxide layer was thinned down to 50 nm by a wet etching in 10:1 buffered oxide etchant (BOE).

(2) EBL was performed on PMMA-coated (thickness $=$ 90 nm) substrate with an area scan mode, a dose of 300 μC cm^{-2}, a working distance of 6 mm, 1500× magnification and an acceleration voltage of 30 kV. Then, the sample was developed in the PMMA developer (isopropyl alcohol (IPA):methyl isobutyl ketone (MIBK) = 3:1) for 70 s and this was followed by soaking in IPA for 60 s and finally rinsing with DI water. The residual PMMA layer was descummed by low power O_2 plasma etching.

(3) A pattern of 15 nm thick chromium (Cr) was created in the nanopatterns of the PMMA by a lift-off process. The Cr layer was later used a mask for the RIE of SiO_2.

(4) A SiO_2 layer was etched by a RIE process in a $CHF_3 + Ar$ environment. After removing the top Cr layer, a 50nm thick Si device layer was etched by the RIE process in an HBr plasma with SiO_2 as the mask layer. Then, the remaining top SiO_2 layer was removed using 10:1 BOE. Finally, a thin SiO_2 layer of 3 nm was grown on the SiNW surfaces at 925 °C for 1 min in a dry O_2 environment.

(5) The Al interconnection was photolithographically defined. Then, the sample was thermally annealed in forming gas (10% H_2/90% N_2) at 400 °C for 30 min.

(6) A PDMS microfluidic channel (width $=$ 100 μm, height $=$ 50 μm) was bonded on the chip for fluidic transport of the sample solution. Also, a plastic leaded chip carrier (PLCC) package was used via wire bonding for electrical connection of the sensor.

For obtaining the geometric characteristics of fabricated silicon nanowires such as linewidth (LW) and line edge roughness (LER), we used a SEM metrology interactive toolbox (SuMMIT, EUV Technology, Inc.) Electrical characterization of the silicon nanowires was carried out by employing an Agilent semiconductor analyzer HP 4155.

The testing setup for the SiNW sensor is shown in figure 1. Sample solutions were supplied to the SiNW sensor at a constant flow rate (0.10–0.50 ml h^{-1}), controlled by syringe pumps. For the pH level detection, we used commercially available color-coded pH buffer solutions from Fisher Scientific, Inc.: the pH $=$ 4 solution was based on potassium hydrogen phthalate with formaldehyde and methyl alcohol as additives; the pH $=$ 7 solution was based on sodium hydroxide, and potassium phosphate monobasic; the pH $=$ 10 solution was based on disodium ethylenediaminetetraacetate dehydrate, potassium carbonate, potassium borate, and potassium hydroxide; other pH level solutions were titrated by mixing these pH buffer solutions and measured using a handheld pH meter (Omega Engineering, Inc.).

3. Results and discussion

3.1. Geometrical characterization of fabricated SiNWs

Various SiNW arrays are presented in figure 2. In general, the actual linewidths (blue dots) in figure 2(A-i) follow well the original design widths (red dotted line). However, for the features larger than 50 nm, the actual widths were smaller than the original design. The average widths of nanowires with $W_{\text{nominal}} = 100$ nm and 150 nm were 88.1 nm (−11.9%) and 135.6 nm (−9.6%), respectively. Possible reasons for this size reduction are errors in the raster control of the electron beam and the shadowing effect of the PMMA resist pattern during the Cr deposition process. Incorrect calibration of the dose

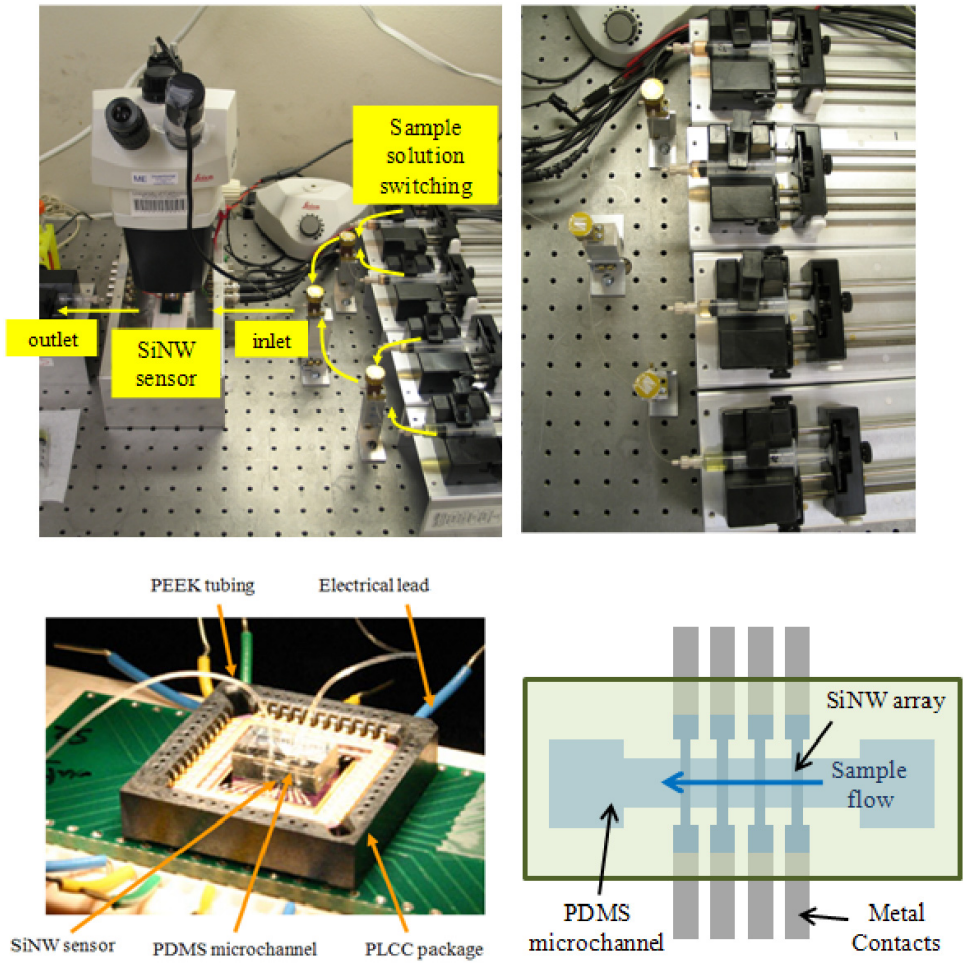

Figure 1. Experimental setup for the SiNW sensor testing: computer-controlled syringe pumps supplied different sample solutions at a fixed flow rate while the samples were manually switched by using a series of selection valves. The fluidic packaging was made by using PDMS-based microchannels and the electrical packaging was made by using a plastic leadless chip carrier (PLCC).

level could also cause reduced exposure to the electron beam resist, resulting in diminished linewidth of features. On the other hand, the features of $W_{\text{nominal}} < 40$ nm were patterned larger than the nominal sizes. These larger dimensions may be due to imperfect focus of the electron beam, overdevelopment of the resist, lateral etching of the PMMA during the O_2 plasma descumming step, and scattering effects of the electron beam [22].

Line edge roughness (LER) was found to be relatively constant, ranging in 5–7 nm regardless of the nominal width (W_{nominal}) of the SiNWs. The effects of LER become evident as the CD gets smaller as shown in figure 2(A-iii,iv). For example, (LER/LW) = (6.6/27.2) = 24.5% for nanowires with $W_{\text{nominal}} = 20$ nm whereas (LER/LW) = (6.2/88.2) = 7.0% for nanowires with $W_{\text{nominal}} = 100$ nm. Therefore the charge transport through SiNWs will be greatly affected by the LER as the dimensions get smaller. Possible causes of LER include the quality of the aerial image [23], the molecular structure of the resist polymers [24], the degree of mixing of the resist components [25] and the development and processing conditions [26, 27]. Firstly, there exists statistical fluctuation of location and dose of incident electrons due to the shot noise effects in the EBL system, causing a fluctuation of electron exposure on the resist across the features. Secondly, the surface of the resist is actually not uniform but consists of higher order structures formed by the aggregation of many polymer molecules [28]. These polymer aggregates were already formed before the EBL process, and thus react differently to the electron beam exposure and dissolve at different rates in the developer. Lastly, the developer solution of a certain concentration and strength can roughen and swell the surface of unexposed area, resulting in the rough line edge.

For sensor application, an array of ten nanowires was fabricated as shown in figure 2(B). The top-down nanofabrication process allowed a perfectly aligned array of parallel nanowires and integration with microwire interconnection via monolithic patterning and etching process, which is very difficult with bottom-up synthesized nanowires.

3.2. Electrical characterization of fabricated SiNWs

The results of current–voltage (I–V) characterization for SiNWs with width (W) = 80, 130 and 300 nm are shown in figure 3. Two major facts were observed from these results. Firstly, the nanowires behave like common ohmic resistors with a linear I–V relation after thermal annealing. The average

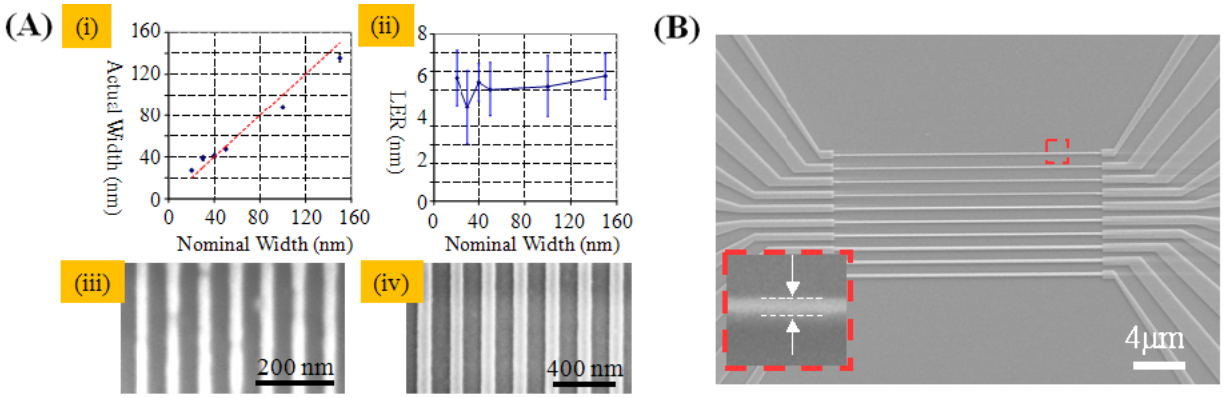

Figure 2. (A) Linewidth (LW) and line edge roughness (LER) of silicon nanowires fabricated by the top-down nanofabrication process (electron beam lithography and reactive ion etching of the silicon on insulator substrate); (B) silicon nanowire sensor arrays fabricated by the top-down nanofabrication process (inset: 50 nm width).

resistance values of nanowires with $W = 80$ nm, 130 nm and 300 nm were 2.56 MΩ, 0.80 MΩ and 0.35 MΩ, respectively. Smaller nanowires have a bigger standard deviation of the resistance due partially to a larger effect of line edge roughness (LER). Secondly, the contact between Al and Si has good ohmic characteristics after the thermal annealing process. The SiNW was moderately doped with a boron (B) concentration of 5×10^{18} cm^{-3}, at which the contact resistance is very high before thermal annealing [29]. However, the thermal annealing process facilitated a good ohmic contact between Al and Si. As shown in figure 3(B), the resistances of the nanowires decreased from 752 MΩ to 2.72 MΩ, from 20.4 MΩ to 0.81 MΩ, and from 2.03 MΩ to 0.38 MΩ for $W = 80$ nm, $W = 130$ nm, and $W = 300$ nm, respectively. The ratio between the electrical conductances before and after the thermal annealing ($S_{\text{annealed}}/S_{\text{as-is}}$) is 56.3, 20.8 and 5.21 for $W = 80$ nm, 130 nm and 300 nm, respectively. If the conductance increase upon thermal annealing was solely due to a better Al–Si contact, ($S_{\text{annealed}}/S_{\text{as-is}}$) would not be such a strong function of the nanowire dimensions. The specific contact resistivity was measured as 6.59×10^{-4} Ω cm^2 before thermal annealing and 1.46×10^{-4} Ω cm^2 after thermal annealing. Therefore, the contact resistance at each contact area was 2.64 kΩ before thermal annealing and 0.58 kΩ after annealing, both of which are much smaller than the total resistance of the SiNW device. From this fact, we can infer that the increase of electrical conductance upon thermal annealing is partially due to better ohmic contact between Al and Si, but mainly due to the conduction enhancement of the SiNW itself. It is conjectured that the organic contaminants around the SiNW and the interface trapped charge (Q_{it}) or the oxide trapped charge (Q_{ot}) developed during the plasma etching process may be reduced during the thermal annealing process [30].

It was also observed that the electrical conductivity (σ) of nanowires is highly dependent on the width of the nanowire. The electrical conductivity for $W = 80$ nm was $\sigma = 70.2$ S m^{-1}, which is much smaller than $\sigma = 1370$ S m^{-1} for $W = 300$ nm. The reasons for this difference can be found from the larger surface effects for smaller nanowires. As mentioned above, the surface damage, defects, and trapped charges can be developed during the plasma etching process. These contamination effects play more significant roles for smaller nanowires due to the larger surface to volume ratio. Also, the ratio of line edge roughness (LER) to linewidth (LW) becomes larger for smaller nanowires. Therefore, electrical conductivity could be reduced by larger surface scattering of mobile charge carriers. The discrepancy between different sizes is reduced after the thermal annealing process, as shown in figure 3(B-iii).

3.3. Real-time pH level detection

SiNW sensors with $W = 100$ nm were used for the real-time detection of four different pH buffer solutions (pH = 4, 6, 8 and 10). The resistance showed the highest value ($R_{\text{avg}} = 2.07$ MΩ) for pH = 4 and the lowest value ($R_{\text{avg}} = 1.79$ MΩ) for pH = 10. The average sensitivity and rise time were $(\Delta R/R)/\Delta\text{pH} = 2.6\%/\text{pH}$ and 7.9 s, respectively. However, when the solution was changed from pH = 6 to pH = 4, the sensor showed very little change of electrical resistance ($R_{\text{avg}} = 2.06$ MΩ for pH = 6 and $R_{\text{avg}} = 2.07$ MΩ for pH = 4). This may be because no more silanol (–SiOH) sites for protonation are available at pH = 4. Another noteworthy fact is the hysteresis in the sensor signal. For example, when the solution is switched from pH = 6 to 4 and then back to 6 again, the average resistances at pH = 6 before and after the pH = 4 solution are $R_{\text{avg}} = 2.06$ MΩ and $R_{\text{avg}} = 2.01$ MΩ, respectively. The same hysteresis effect is observed for pH = 8. In the sequence of decreasing pH (pH = 10 → 8 → 6 → 4), the average resistance is $R_{\text{avg}} = 1.937$ MΩ. On the other hand, in the sequence of increasing pH (pH = 4 → 6 → 8 → 10), the average resistance is $R_{\text{avg}} = 1.869$ MΩ. This hysteresis is believed to be caused by the presence of buried OH sites just below the surface [31] and shift in the point of zero charge (pH_{pzc}) [32]. Water (H_2O) diffuses into thin SiO_2 layers with a low activation energy, even at room temperature [33]. Most of this H_2O reacts with the SiO_2 structure and forms Si–OH sites at a concentration in the 10^{19}–10^{20} cm^{-3} range near the surface of SiO_2 [33]. These Si–OH sites slowly react with H^+ ions from the solution with

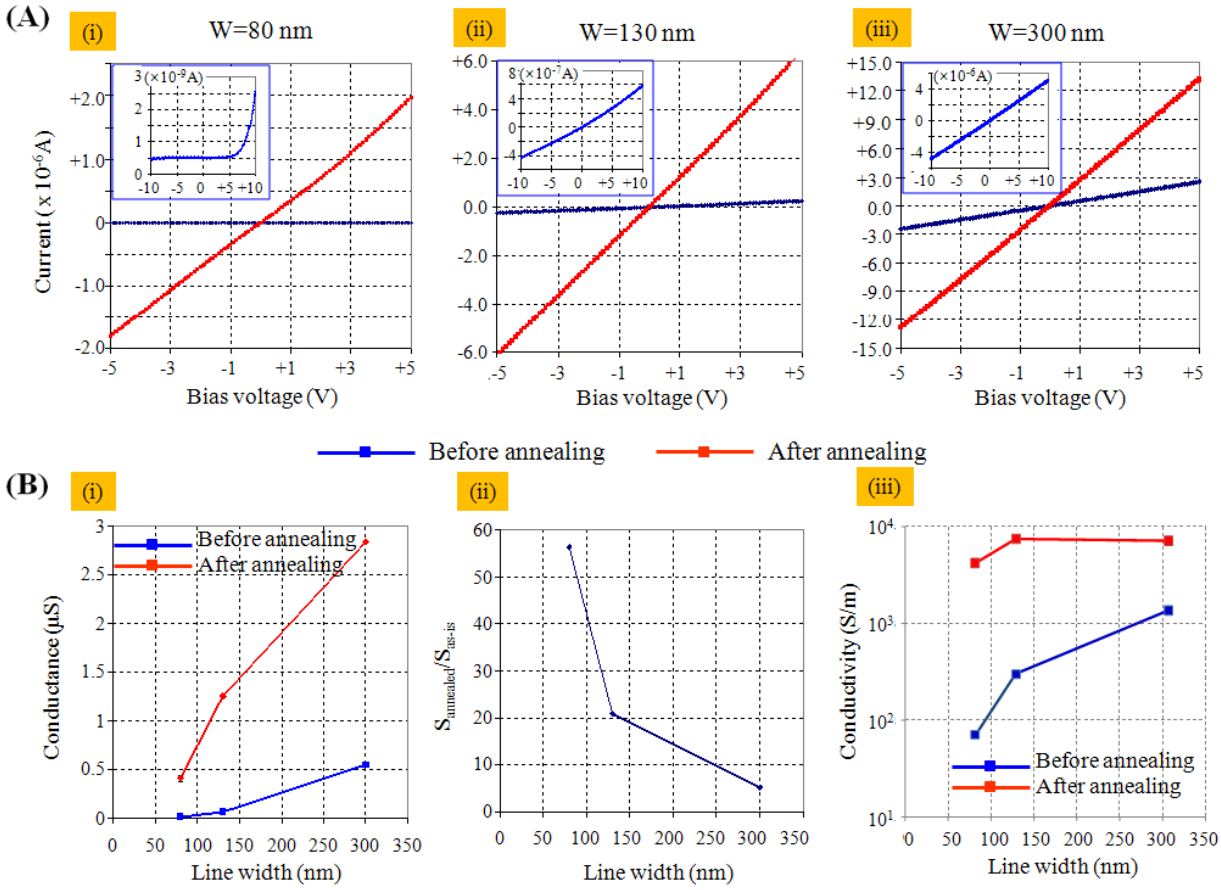

Figure 3. Electrical characterization of silicon nanowires: (A) statistical analysis of the electrical resistivity of silicon nanowires (length $L = 40$ μm, thickness $h = 50$ nm, width $W = 80, 130, 300$ nm), (B) effect of thermal annealing on the I–V characteristics of SiNWs in various sizes of silicon nanowires.

long time constants. Although this number of Si–OH sites buried below the surface is small compared to the number of sites on the surface, the slow response of these buried sites to the electrolyte pH level changes is believed to be the source of hysteresis during the sample solution switching. If the pH level of sample solution is changed, the point of zero potential (pH_{pzc}) of the surface of SiO_2 is slightly modified [32]. When the pH level of the solution is continuously switched, pH_{pzc} is altered and the response of the SiNW is changed as a consequence. This can cause hysteresis in the sensor signals.

Despite the existence of hysteresis and overshoot in the SiNW sensor, it is still sensitive enough and has enough reproducibility to detect small pH level changes near the neutral pH level (pH = 7). The real-time pH level detection when switching the solutions among pH = 6.7, 6.9, 7.1 and 7.3 every 90 s is shown in figure 4(B). The average sensitivity and rise time of the sensor response were $(\Delta R/R)/\Delta\text{pH} = 3.6\%/\text{pH}$ and 8.5 s, respectively. Here, we could also observe initial spikes during sample switching and hysteresis of sensor signals at each pH level. The plot of average resistance (R_{avg}) versus pH level in figure 4(C) shows a linear relationship between the pH level and average resistance. The average signal to noise ratio (SNR) was 8.3, which implies that we can potentially detect an even smaller pH level difference down to 0.05 by using the SiNW sensor. The performance of our SiNW sensors in terms of resolution and detection speed renders them good tools for the real-time *in vitro* extracellular pH measurement of single cells. For example, when antibody-mediated crosslinking occurs on the surface of T-cells, they get activated and intracellular signaling drives the release of acid in the extracellular environment [34, 35]. The local change of pH level in this case is known to be $\Delta\text{pH} \approx -0.4$ in a response time of about 3 min. Therefore, our SiNW sensor should provide sufficient sensitivity and response speed for this kind of *in vitro* single-cell measurement.

To explore the size effect of SiNWs on their sensitivity to the pH level changes, nanowires with two different widths (100 and 200 nm) were compared. The thickness and length of the nanowires were the same, at 50 nm and 20 μm, respectively. As shown in figure 4(D), the nanowire with 100 nm width showed higher sensitivity ($(\Delta R/R) = 16\%$ for $\Delta\text{pH} = 6$) than that with 200 nm width ($(\Delta R/R) = 13\%$ for $\Delta\text{pH} = 6$). The modulation of the electrical resistance in the silicon nanowire is based on the change of surface potential and formation of a depletion layer on the surface of the nanowire when charged molecules are attached. Therefore the sensitivity is highly affected by the surface to volume ratio. Theoretical analysis of the dependence of the sensitivity to the geometry of the nanowire is given in another paper by the author [11]. In short, the relative change of electrical conductance of p-type

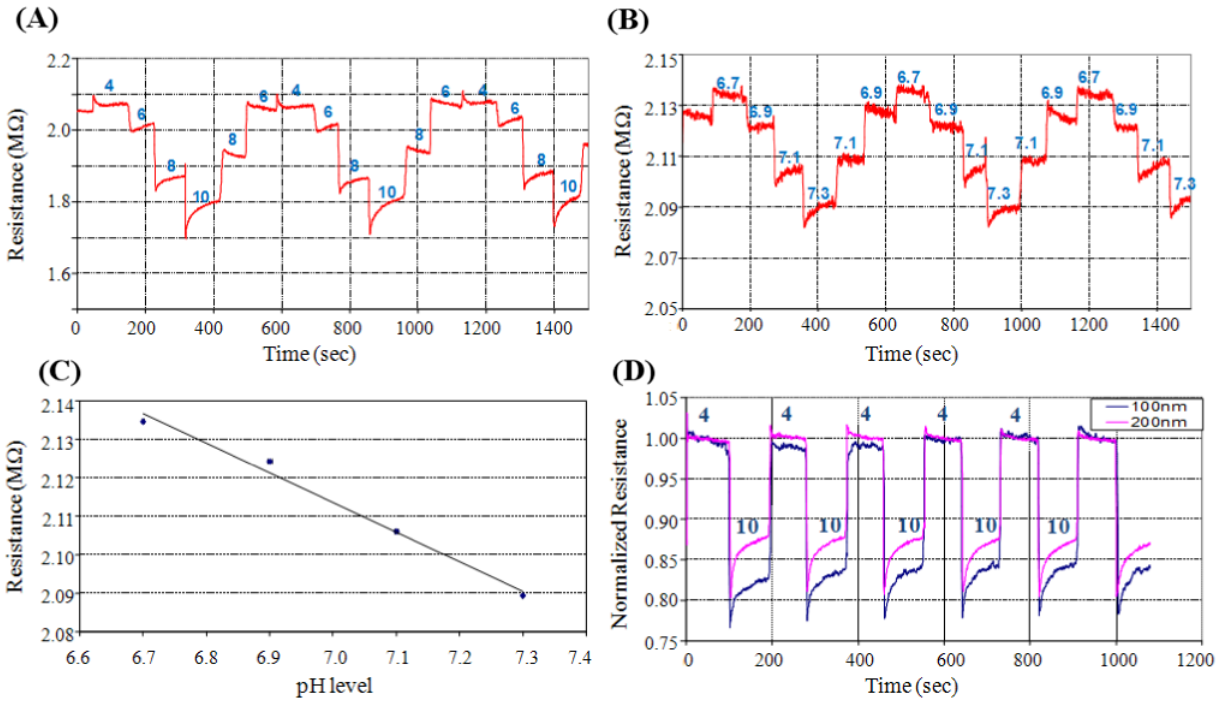

Figure 4. Result of real-time pH level detection by the SiNW sensor; (A) pH level switching between pH = 4, 6, 8, and 10 every 90 s, (B) pH level switching between pH = 6.7, 6.9, 7.1, and 7.3 every 90 s, (C) average resistance versus pH level near the neutral pH level, (D) size dependence of the sensitivity to the width of silicon nanowires (W = 100 and 200 nm).

doped silicon nanowire can be derived as

$$\frac{\Delta S}{S} \approx -\frac{(W+2H)}{WH} \cdot \frac{N_S}{N_A}$$

where S is the electrical conductance, W and H are the width and thickness of the nanowire, N_S is the concentration of surface charge, and N_A is the concentration of doping impurity within the nanowire. Here, the first term $(W + 2H)/WH$ represents the surface to volume ratio of the nanowire. This equation shows that the sensitivity of the nanowire sensor increases when the surface charge concentration increases, the dopant concentration within the nanowire decreases, and the cross-sectional size of the nanowire decreases. This equation predicts the sensitivity ratio between 100 and 200 nm wide nanowires to be 1.33, assuming the same level of surface charge density in the two nanowires, whereas the experimental result gives 1.23. This error may be due to assumptions in the model (uniform doping concentration within the nanowire and depletion region thickness much smaller than the width and thickness of the nanowire) and the effects of other resistance components (silicon–metal contact resistance, silicon microwire interconnection, metal interconnection, etc). Nonetheless, the experimental result clearly shows that a smaller nanowire has higher sensitivity through a high surface to volume ratio.

3.4. Sensitivity to alkali metal ions

In section 3.3, pH buffer solutions with certain ionic species and strength were used for the pH level detection. In more realistic applications of chemical detection, a sensor may encounter other components in the sample solution—organic contaminants, inorganic particles and metallic ions. In particular, electrolyte solutions with alkali metallic ions such as sodium (Na^+) and potassium (K^+) ions are common conditions for biochemical sensing. Therefore, the characterization of sensitivity of SiNW sensors to these metal ions present in the sample solutions is of great importance.

The result of the sensitivity of the SiNW sensor to the potassium chloride (KCl) dissolved in the pH = 7 buffer solution is shown in figure 5(A-i). The sensor showed an increase of resistance when the sample was switched from a pH = 7 buffer solution without additional KCl salts to the same solution with KCl added. For 1 M, 0.1 M and 0.01 M of KCl, the resistance increased from R = 2.26 MΩ to R = 2.36 MΩ (+4.4%), 2.29 MΩ (+1.3%) and 2.28 MΩ (+0.6%), respectively. For the concentration of 0.001 M, the signal was not obvious compared to the noise level. Similar results were observed for the sodium chloride (NaCl), as shown in figure 5(A-ii).

The sensitivity of SiNW to the metal ions can be explained by the selective adsorption of positive metallic ions (K^+ and Na^+) on the surface of SiNW. The point of zero charge (pH_{pzc}) for SiO_2 is in the range of pH = 1–4 [36–38] depending on the processing conditions and properties of the film. Since the measurements in figure 5(A) were made at pH = 7, the surface charge on the SiNW would be negative. This can be expressed as the following equation of chemical reaction:

$$\equiv\text{Si–OH} + \text{OH}^- \leftrightarrow \equiv\text{Si–O}^- + \text{H}_2\text{O}.$$

In the electrolyte solution, an electrical double layer (EDL) is formed and positive counterions will be accumulated

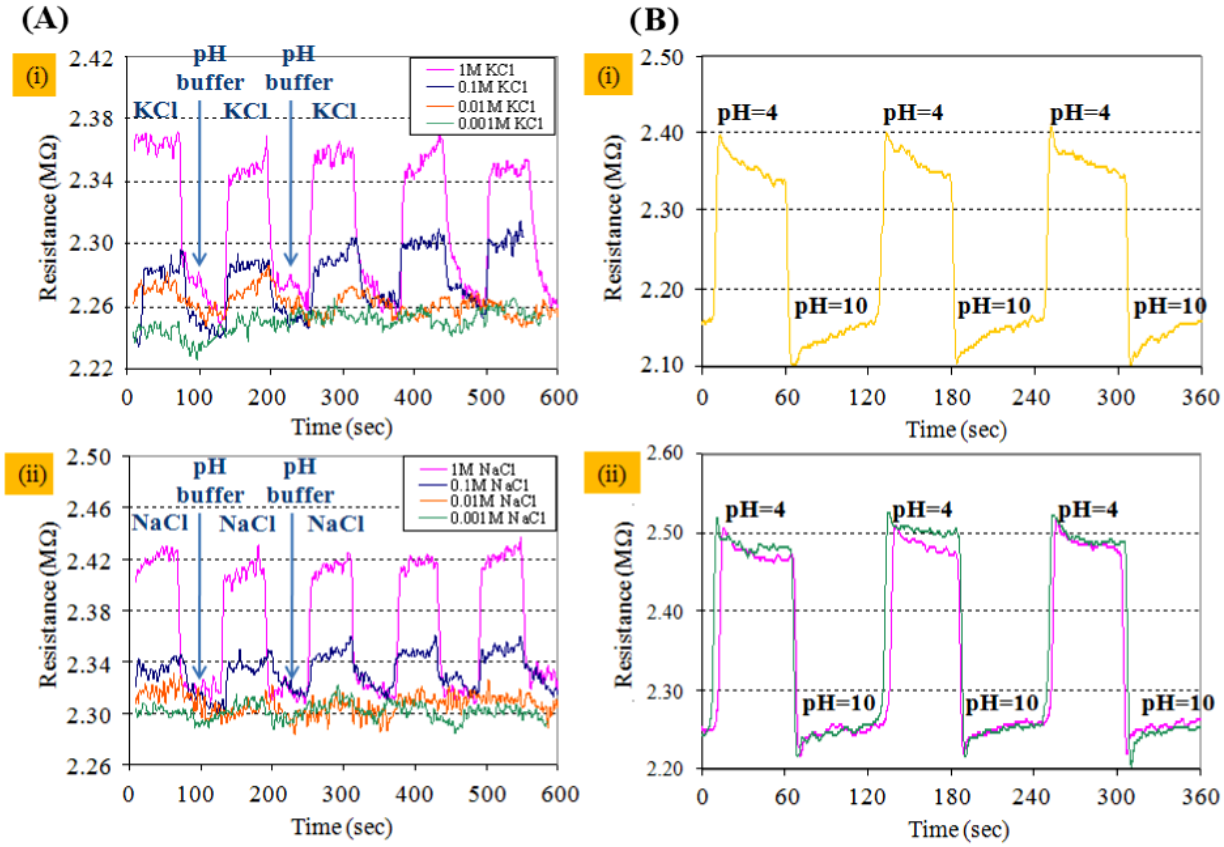

Figure 5. Sensitivity of the silicon nanowire sensor to alkali metal ions. (A) Response to potassium chloride (KCl) and sodium chloride (NaCl) dissolved in pH = 7 buffer solution. (B) Real-time pH level (4 and 10) detection (i) without and (ii) with the presence of alkali metal ions (green curve: 1 M KCl, magenta curve: 1 M NaCl).

within this layer by the electrostatic attraction from negatively charged silicon surface [39]. Therefore K^+ or Na^+ ions are selectively (compared to Cl^- ions) attracted to the surface of SiNW and react with the SiO_2 surface in the following reaction:

$$\equiv\text{Si–O}^- + \text{Na}^+ \leftrightarrow \equiv\text{Si–O–Na};$$

$$\equiv \text{Si–O}^- + \text{K}^+ \leftrightarrow \equiv\text{Si–O–K}.$$

This selective binding of positive metal ions (Na^+) compared to the Cl^- ions at the neutral pH level has been experimentally verified by x-ray photoelectron spectroscopy (XPS) study in the literature [40]. According to the paper [40], at the neutral pH level where the surface charge of SiO_2 is negative, more Na elements than Cl elements were detected since Na^+ counterions were accumulated in the electrical double layer. Accumulation of more positive ions (Na^+ or K^+) causes depletion of mobile charge carriers (holes) in the p-type silicon and increased electrical resistance as a consequence.

Although the existence of alkali metal ions (Na^+ or K^+) affected the electrical resistance of SiNWs, changes of pH levels could still be detected. Figure 5(B) shows the comparison of real-time pH level detection results for as-received pH buffer solutions (orange curve) and for the same solutions with 1.0 M Na^+ (magenta curve) and K^+ (green curve) added. The resistance was increased by $\Delta R \approx 0.10$ MΩ by the addition of both Na^+ and K^+. However, the sensitivity of the SiNW sensor showed only small changes. Detection for pH buffer solutions (with no additional alkali ions) and solutions with 1 M Na^+ and K^+ added exhibited $\Delta R/R = 10.9\%, 10.3\%$ and 12.2% for $\Delta\text{pH} = 6$. This indicates that the alkali ions in the electrical double layer do not block the access of proton (H^+) ions to the surface of SiO_2 on the nanowire, so protonation and deprotonation can occur upon change of the pH level. Thus, pH level detection can be carried out as long as the concentrations of other alkali metal ions are kept constant.

3.5. Long term stability of SiNW sensors

Long term stability is of crucial importance if the SiNW sensor is to be deployed in practical applications that require continuous monitoring of chemical species for long periods of time. For example, continuous monitoring of the blood pH level during surgery requires a sensor with an accuracy of 0.02 pH unit over a period of 10 h without the need for calibration [41]. However the experimental results showed that the SiNW sensor is not very stable in long term operation. The electrical resistance of a SiNW sensor (width = 100 nm) was monitored under a constant flow of pH buffer solutions (flow rate $Q = 0.3$ ml h^{-1}) for 8 h. The results for three different pH buffer solutions at pH = 4, 7 and 10 are shown in figure 6.

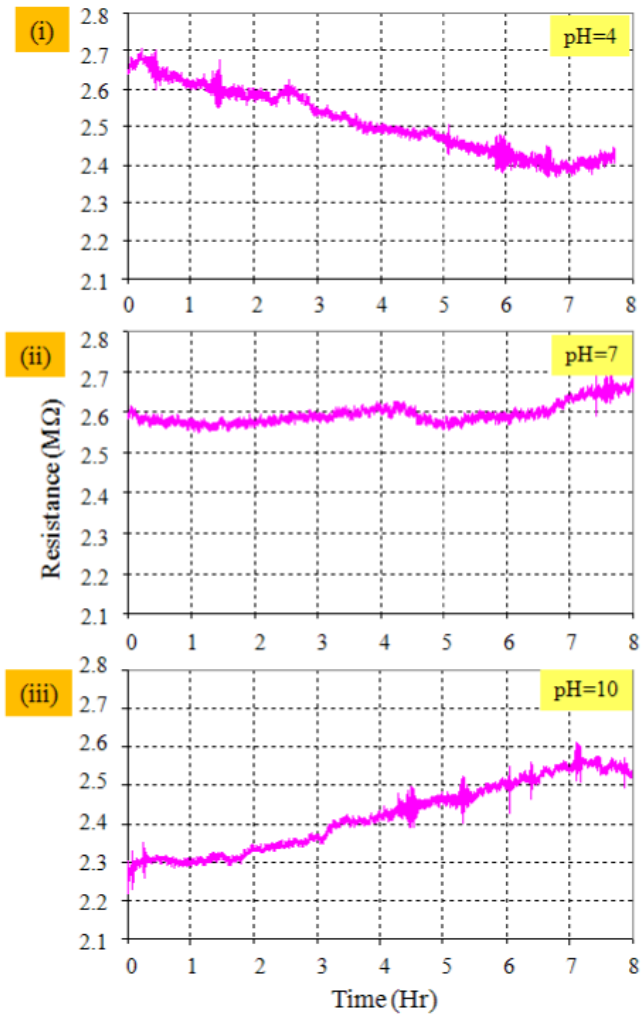

Figure 6. Long term stability analysis of silicon nanowire sensors at (i) pH = 4, (ii) pH = 7, and (iii) pH = 10.

Short term fluctuations and long term drift were observed for various pH solutions. At pH = 4, the resistance of the SiNW sensor gradually decreased from $R = 2.65$ to 2.40 MΩ over 7 h. Except for short periods ($t = 2.3$–2.5 h; $t = 4.6$–4.8 h), the nanowire sensor showed a monotonic decrease of the resistance. At pH = 7, the resistance of the nanowire showed little change, the resistance only increasing slightly from $R = 2.59$ to 2.64 MΩ over 7 h. At pH = 10, the resistance gradually increased from $R = 2.25$ to 2.55 MΩ over 7 h.

These drift effect is a very common deficient characteristic of pH sensors, especially ion sensitive field effect transistors (ISFET). Several mechanisms for this drifting phenomenon have been proposed in the literature: slow hydration of the SiO_2 surface [42], ion exchange of OH^- ions and incorporation in the solid [43], injection of electrons from electrolyte into the SiO_2 surface [31, 44], and migrations of ions such as H^+ and OH^- into the surface [45, 46]. Although several causes of signal drift have been proposed and verified, most of these studies have been performed at near neutral pH levels. From our experiments, we found that the drifting occurs in different directions for acid and base solutions. In low pH (pH = 4) buffer solution, resistance decreases monotonically. It is speculated that this is likely due to the accumulation of negative charges on the surface of SiO_2. This slowly decreases the depletion effect and reduces the resistance as a consequence. On the other hand, at a high pH (pH = 10) level, resistance continuously increases. This is likely due to a slow etching of silicon (Si) by potassium hydroxide (KOH) and potassium carbonate (K_2CO_3) which are present at 0.6% and 0.2%, respectively in the pH = 10 buffer solution. KOH is a strong etchant for Si (1100 nm min^{-1} for Si(100) at 80 °C by 30 wt% KOH) and also etches SiO_2 at a slow rate (6.7 nm min^{-1} at 80 °C) for a concentration of 30% by weight in DI water [47]. Even though their concentrations are very low, they can slowly dissolve SiO_2 and Si over a very long period of time. This slow etching results in reduction in size of the nanowire and thus the resistance increases.

Researchers have found that SiO_2 is not a very stable insulator material for ion sensitive field effect transistor (ISFET) use in terms of hysteresis and drift. Alternative materials such as Si_3N_4 and Al_2O_3 [48] have been proposed as insulators for sensors with improved stability. They not only offer more resistance against ionic diffusion and electron injection in the electrolyte environment but also are less susceptible to being affected by the etching components like KOH.

4. Conclusion

In this work, silicon nanowires (SiNWs) were fabricated by a top-down fabrication approach, integrated with microfluidics, and then tested as chemical sensors for the solution pH level. The high sensitivity and fast response time of the SiNW sensor allowed real-time detection of the solution pH level. The average sensitivity of the SiNW was found to be approximately $(\Delta R/R)/(\Delta \text{pH}) \approx 3.0\%/\text{pH}$. The average rise time was below 8 s. However, the intrinsic response time of the SiNW sensor itself is expected to be much shorter as regards the mixing and diffusion time within the microfluidic channel. The stability and high sensitivity allowed real-time detection of small pH level changes down to $\Delta\text{pH} = 0.2$ with signal to noise ratio larger than 8. The sensor showed a good linear relation between the resistance and pH level near neutral pH (pH = 7), but the linearity was broken in a larger pH range (pH = 4–10) due to lack of further binding sites for proton ions (H^+) in the low pH regime. The SiNW sensor exhibited sensitivity not only to the pH levels but also to the concentration of alkali metal ions such as sodium (Na^+) and potassium (K^+) ions. Even though the sensor does not have selectivity for these ions at the current stage, it is expected that surface modification of nanowire with metal–ion sensitive molecules such as crown ethers would allow selective detection of metal ions. The long term stability result for SiNWs at a constant pH level revealed a drift in the electrical resistance with a slope dependent on the pH level. This long term instability and short term hysteresis of the SiNW sensor will motivate future development of surface protection layers (Si_3N_4 or Al_2O_3) or compensation via an electrical circuit or software.

It is expected that the top-down fabricated SiNW sensors, if the performance factors discussed here are improved, will find a number of applications in various areas such as environmental sensing, *in vitro* single-cell analysis, and biomedical monitoring devices.

Acknowledgments

The authors would like to express their gratitude for the generous financial support by the Center for Nanoscale Mechatronics and Manufacturing (CNMM; Grant No. 019997), the Basic Research Support Program (Grant No. 2009-0069838) of the Ministry of Education, Science, and Technology in Korea and Hewlett-Packard (HP) Company.

References

[1] Samitsu S, Shimomura T, Ito K, Fujimori M, Heike S and Hashizume T 2005 *Appl. Phys. Lett.* **86** 233103
[2] Wanekaya A K, Bangar M A, Yun M, Chen W, Myung N V and Mulchandani A 2007 *J. Phys. Chem.* C **111** 5218
[3] Ramanathan K, Bangar M A, Yun M, Chen W, Mulchandani A and Myung N V 2004 *Nano Lett.* **4** 1237
[4] Yeong K S, Maung K H and Thong J T L 2007 *Nanotechnology* **18** 185608
[5] Zhang D, Liu Z, Li C, Tong T, Liu X, Man S, Lei B and Zhou C 2004 *Nano Lett.* **4** 1919
[6] Morante J R, Baratto C, Comini E, Faglia G, Ferroni M, Ponzoni A and Vmiero A 2007 *Sensors Actuators* B **121** 3
[7] Li Q, Zhu X, Xiong H D, Koo S M, Ioannou D, Kopanski J J, Suehle J S and Richter C A 2007 *Nanotechnology* **18** 4
[8] Zheng G, Lu W, Jin S and Lieber C M 2004 *Adv. Mater.* **16** 1890
[9] Li Z, Chen Y, Li X, Kamins T, Nauka K and Williams R S 2004 *Nano Lett.* **4** 245
[10] Li Z, Rajendran B, Kamins T, Li X, Chen Y and Williams R S 2005 *Appl. Phys.* A **80** 1257
[11] Park I, Li Z, Li X, Pisano A P and Williams R S 2007 *Biosens. Bioelectron.* **22** 2065
[12] Park I, Li Z, Pisano A P and Williams R S 2007 *Nano Lett.* **7** 3106
[13] Cui Y, Wei Q Q, Park H and Lieber C M 2001 *Science* **291** 630
[14] Wang W U, Chen C, Lin K H, Fang Y and Lieber C M 2005 *Proc. Natl Acad. Sci.* **102** 3208
[15] Li C, Curreli M, Lin H, Lei B, Ishikawa F N, Datar R, Cote R J, Thompson M E and Zhou C 2005 *J. Am. Chem. Soc.* **127** 12484
[16] Zheng G, Patolsky F, Cui Y, Wang W U and Lieber C M 2005 *Nat. Biotechnol.* **23** 1294
[17] Wissner-Gross A D 2006 *Nanotechnology* **17** 4086
[18] Fan Z, Ho J C, Jacboson Z A, Yerushalmi R, Alley R, Razavi H and Javey A 2008 *Nano Lett.* **8** 20
[19] Pauzauskie P, Radenovic A, Trepagnier E, Shroff H, Yang P and Liphardt J 2006 *Nat. Mater.* **5** 97
[20] Molhave K, Hansen T M, Madsen D N and Boggild P 2004 *J. Nanosci. Nanotechnol.* **4** 279
[21] Elibol O H, Morisette D, Akin D, Denton J P and Bashir R 2003 *Appl. Phys. Lett.* **83** 4613
[22] Suzuki K, Matsui S and Ochiai Y 2000 *Sub-Half-Micron Lithography for ULSIs* (Cambridge: Cambridge University Press)
[23] Yoshizawa M and Moriya S 2000 *Proc. SPIE* **3997** 301
[24] Yamamoto J, Uchino S, Hattori T, Yoshimura T and Murai F 1996 *Japan. J. Appl. Phys.* **35** 6511
[25] McKean D, Allen R, Kasai P, Schaedeli U and MacDonald S 1992 *Proc. SPIE* **1672** 94
[26] Dobisz E A, Brandow S L, Snow E and Bass R 1997 *J. Vac. Sci. Technol.* B **15** 2318
[27] Yoshimura T, Shiraishi H, Yamamoto J and Okazaki S 1993 *Appl. Phys. Lett.* **63** 764
[28] Yamaguchi T, Yamazaki K, Nagase M and Namatsu H 2003 *Japan. J. Appl. Phys.* **42** 3755
[29] Zant P V 2004 *Microchip Fabrication* 5th edn, McGraw-Hill Professional
[30] Franssila S 2004 *Introduction to Microfabrication* (New York: Wiley)
[31] Bousse L and Bergveld P 1984 *Sensors Actuators* B **6** 65
[32] Bousse L, Mostarshed S and Hafeman D 1992 *Sensors Actuators* B **10** 67
[33] Pfeffer R, Lux R, Berkowitz H, Lanford W A and Burman C 1982 *J. Appl. Phys.* **53** 4226
[34] Beeson C, Rabinowitz J, Tate K, Gutgetmann I, Chien Y H, Jones P P, Davis M M and McConnell H M 1996 *J. Exp. Med.* **184** 777
[35] McConnell H M, Wada H G, Arimilli S, Fok K S and Nag B 1995 *Proc. Natl Acad. Sci.* **92** 2750
[36] Fung C D, Cheung P W and Ko W H 1986 *IEEE Trans. Electron. Dev.* **33** 3
[37] Bousse L J, Mostarhed S, Shoot B, De Rooij N F, Gimmel P and Gopel W 1991 *J. Colloid. Interface Sci.* **147** 22
[38] Raiteri R, Margesin B and Grattarola M 1998 *Sensors Actuators* B **46** 126
[39] Sonnefeld J, Göbel A and Vogelsberger W 1995 *Colloid Polym. Sci.* **273** 926
[40] Shchukarev A V 2007 *Colloid J.* **69** 514
[41] Bergveld P and Sibbald A 1988 *Comprehensive Analytical Chemistry* vol XXIII (Amsterdam: Elsevier)
[42] Iler R K 1979 *The Chemistry of Silica* (New York: Wiley)
[43] Berube Y G, Onoda G Y and de Bruyn P L 1967 *Surf. Sci.* **7** 448
[44] Nicollian E H, Berglund C N, Schmidt P F and Andrews J M 1971 *J. Appl. Phys.* **42** 5654
[45] Esashi M and Matsuo T 1978 *IEEE Trans. Biomed. Eng.* **25** 184
[46] Topkar A and Lal R 1993 *Thin Solid Films* **232** 265
[47] Williams K R, Gupta K and Wasilik M 2003 *J. Microelectromech. Syst.* **12** 761
[48] Jamasb S, Collins S D and Smith R L 1998 *IEEE Trans. Electron. Dev.* **45** 1239